Toward a unified modeling of environment and bridge-mediated contributions to electronic energy transfer: a fully polarizable QM/MM/PCM approach

Stefano Caprasecca,*,† Carles Curutchet,*,‡ and Benedetta Mennucci*,†

Dipartimento di Chimica e Chimica Industriale, University of Pisa, Via Risorgimento 35, 56126 Pisa, Italy, and Departament de Fisicoquímica Facultat de Farmàcia, Universitat de Barcelona Av. Joan XXIII s/n, 08028 Barcelona, Spain

E-mail: stefano.caprasecca@for.unipi.it; carles.curutchet@ub.edu; bene@dcci.unipi.it

Abstract

Recent studies have unveiled the similar nature of solvent (screening) effects and bridge-mediated contributions to electronic energy transfer, both related to the bridge/solvent polarizability properties. Here we exploit the similarity of such contributions to develop a fully polarizable mixed QM/discrete/continuum model aimed at studying electronic energy transfer processes in supramolecular systems. In the model, the definition of the three regions is completely flexible and allows us to explore the possibility to describe bridge-mediated contributions by using a polarizable MM description of the linker. In addition, we show that the classical MMPol description of the bridge can be complemented either with an analogous atomistic or a continuum description of the solvent. Advantages and drawbacks of the model are finally presented and discussed with respect to the system under study.

*To whom correspondence should be addressed

†Dipartimento di Chimica e Chimica Industriale, University of Pisa, Via Risorgimento 35, 56126 Pisa, Italy

‡Departament de Fisicoquímica Facultat de Farmàcia, Universitat de Barcelona Av. Joan XXIII s/n, 08028 Barcelona, Spain

1 Introduction

Electronic energy transfer (EET) consists in the radiationless migration of the excitation energy of a sensitized donor (D) to a proximate acceptor (A). In photosynthesis, ultrafast EET among antenna pigment-protein complexes allows to funnel the captured sunlight to reaction centers with very high quantum efficiencies.[1–4] The same principle is used in organic photovoltaic cells, where the absorbed excitons have to be efficiently transferred to charge-separation interfaces,[5,6] whereas in organic light-emitting diodes (OLED) the processes is reversed, and EET is used to direct the excitons generated upon charge injection.[7,8]

The basic design principles of EET processes can be understood based on Förster theory,[9] which relates the transfer rate between weakly coupled D/A molecules with the square of the electronic coupling matrix element between the initial and final states of the EET reaction, V, and a spectral overlap factor between normalized donor emission and acceptor absorption lineshapes, J:

$$k = \frac{2\pi}{\hbar} V^2 J, \tag{1}$$

In intermolecular EET, the effect of the molecular environment on the electronic coupling V is typically described in terms of a screening effect that significantly slows down the EET process. In Förster theory, this effect is described by a rather crude screening factor $s = 1/n^2$, where n is the refractive index of the medium, so that the total coupling is cast in terms of a direct D/A interaction V_s and a screening factor s, $V = s \cdot V_s$. In intramolecular EET processes, however, the D/A units are covalently linked by some molecular spacer that can significantly modulate the coupling between the units,[10–12] in so-called through-bond contributions either mediated by superexchange, as in electron transfer,[13,14] or by modifying the D/A Coulombic interaction.[12]

In the last decade there have been important efforts in order to accurately model both screening effects[15–23] and bridge-mediated effects to EET.[24–31] Screening effects, which arise from the coupling of solvent electronic states with the D/A states,[20] can be modeled either using continuum dielectric models, mixed quantum mechanics/molecular mechanics (QM/MM) methods, or

by including them in the QM calculation as in subsystem TDDFT.[21,32] In continuum models, the solvent contribution is dictated by its macroscopic optical dielectric constant, i.e. approximately the refractive index related to the solvent polarizability,[33] whereas in mixed QM/MM models solvent molecules are explicitly considered and described through a classical polarizable force field.[19] Bridge-mediated effects, on the other hand, arising from coupling of the bridge states to the D/A states, are typically modeled by including the linker in the QM calculation.[24–31] Recent studies, however, have pointed out that the leading contributions to bridge-mediated singlet-singlet EET often arise from Coulomb contributions rather than superexchange,[27,28,30,31] thus relating the enhancement or screening of the D/A coupling with the bridge polarizability.[28,30]

In the present study, we develop a fully coupled QM/discrete/continuum method for energy transfer that combines a continuum dielectric description of the environment with a flexible definition of QM and polarizable MM regions. This three-level method allows us to explore the possibility to describe bridge-mediated contributions by using a polarizable MM description of the linker combined with a continuum model for solvent effects. In addition, we show that the classical MMPol description of the bridge can be complemented either with an atomistic or a continuum description of the solvent, and discuss some of the advantages and drawbacks of these two options depending on the chemical system under study. Applications to different D-bridge-A systems are reported to determine potentials and limitations of the method.

2 Theory

We implemented a fully polarizable mixed QM/discrete/continuum model, where a solute, described at QM level, is surrounded by a set of polarizable MM atoms and by a polarizable structureless medium. The latter is treated with the Polarizable Continuum Model (PCM),[34] implemented according to the Integral Equation Formalism (IEF-PCM[35,36]), while the MM atoms are represented as a set of charges and induced dipoles, using the MMPol model recently developed by some of the present authors.[19] This MM layer may be employed to describe both solvent molecules

and non-QM parts of the solute itself. Here below we first report the main elements of the general implementation (which is similar to the one presented by Steindal et al.[37]), and successively we detail on its extension to describe EET processes within a TD-DFT formalism.

2.1 The electrostatic problem

In the PCM model, the polarization of the solvent is represented by placing a set of "apparent" charges, $\{q_i^{\mathrm{PCM}}\}$, on the mesh of the molecular cavity's surface. These charges are obtained from the electrostatic potential of the QM solute, plus eventually the potential generated by the MM distribution, using the equation:

$$\boldsymbol{T}\boldsymbol{Q} = \boldsymbol{R}\boldsymbol{V}, \tag{2}$$

where $\boldsymbol{Q}$ is the vector containing the $\{q_i^{\mathrm{PCM}}\}$ set of PCM charges on each of the N_{tes} surface finite elements (generally called "tesserae"), $\boldsymbol{V}$ a vector with the value of the potential on the same tesserae, and $\boldsymbol{T}$ and $\boldsymbol{R}$ are matrices depending on geometrical factors and on the solvent permittivity ε (either the static or the optical one, depending on the case).

On the other hand, the MM molecules are described as a set of fixed charges, $\{q_i^{\mathrm{MM}}\}$, centered on the atoms, and a set of induced dipoles, $\{\boldsymbol{\mu}_i\}$, whose positions are generally referred to as polarizable sites. The induced dipoles can be obtained, similarly to the PCM case, from the electrostatic field due to the QM solute and the PCM and MM distributions, calculated on the polarizable sites:

$$\boldsymbol{M} = \boldsymbol{\alpha}\boldsymbol{E}, \tag{3}$$

where $\boldsymbol{M}$ is the vector containing the induced dipoles $\{\boldsymbol{\mu}_i\}$ on the N_{pol} polarizable sites, $\boldsymbol{E}$ the value of the electric field on the same sites and $\boldsymbol{\alpha}$ the MMPol matrix containing the polarizability tensors $\{\boldsymbol{\alpha}_i\}$ and whose expression depends on the MMPol model used.

Eq. Eq. (2) and Eq. (3) differ from the standard PCM and MMPol equations in that the potential and electric field also contain "mixed" contributions from both the MMPol and PCM distributions, and therefore the two problems cannot be separated.

In more detail, the elements of the total potential of Eq. (2) can be written as:

$$V_t = V_t^{\mathrm{QM}} + V_t^{\mathrm{MM}} = V_t^{\mathrm{QM}} + \sum_c \frac{q_c^{\mathrm{MM}}}{|\boldsymbol{r}_t - \boldsymbol{r}_c|} + \sum_p \frac{\boldsymbol{\mu}_p \cdot (\boldsymbol{r}_t - \boldsymbol{r}_p)}{\left|\boldsymbol{r}_t - \boldsymbol{r}_p\right|^3}$$
$$= V_t^{\mathrm{QM}} + b_t + \sum_p \boldsymbol{S}_{t,p}\boldsymbol{\mu}_p, \tag{4}$$

where indices t, c and p label tesserae, MM charge sites and polarizable sites, respectively.

Similarly, the electric field on each polarizable site, appearing in Eq. (3), can be expressed as:

$$\boldsymbol{E}_p = \boldsymbol{E}_p^{\mathrm{QM}} + \boldsymbol{E}_p^{\mathrm{MM}} + \boldsymbol{E}_p^{\mathrm{PCM}}, \tag{5}$$

where

$$\boldsymbol{E}_p^{\mathrm{MM}} = \sum_c \frac{q_c^{\mathrm{MM}}(\boldsymbol{r}_p - \boldsymbol{r}_c)}{\left|\boldsymbol{r}_p - \boldsymbol{r}_c\right|^3} + \sum_{p' \neq p} \frac{3(\boldsymbol{\mu}_{p'} \cdot \hat{\boldsymbol{r}}_{p,p'})\hat{\boldsymbol{r}}_{p,p'} - \boldsymbol{\mu}_{p'}}{\left|\boldsymbol{r}_p - \boldsymbol{r}_{p'}\right|^3}$$
$$= \boldsymbol{a}_p + \sum_{p' \neq p} \boldsymbol{P}_{p,p'}\boldsymbol{\mu}_{p'} \tag{6}$$

and

$$\boldsymbol{E}_p^{\mathrm{PCM}} = \sum_t \frac{q_t^{\mathrm{PCM}}(\boldsymbol{r}_p - \boldsymbol{r}_t)}{\left|\boldsymbol{r}_p - \boldsymbol{r}_t\right|^3} = \sum_t \boldsymbol{U}_{p,t} q_t^{\mathrm{PCM}}. \tag{7}$$

Substituting the total potential and electric field into Eq. (2) and Eq. (3), and using a more compact matrix form, one can write:

$$\begin{cases} (\boldsymbol{\alpha}^{-1} - \boldsymbol{P})\boldsymbol{M} - \boldsymbol{U}\boldsymbol{Q} = \boldsymbol{E}^{\mathrm{QM}} + \boldsymbol{a} \\ -\boldsymbol{R}\boldsymbol{S}\boldsymbol{M} \qquad + \boldsymbol{T}\boldsymbol{Q} = \boldsymbol{R}\left(\boldsymbol{V}^{\mathrm{QM}} + \boldsymbol{b}\right) \end{cases}, \tag{8}$$

where the Eq. (8) must be solved simultaneously. Noting that $\boldsymbol{a}$ and $\boldsymbol{b}$ are respectively the electric field and potential due to the MM charges, and that $\boldsymbol{S} = -\boldsymbol{U}^{\dagger}$, the system of equations can be

rearranged as:

$$\begin{pmatrix} \boldsymbol{M} \\ \boldsymbol{Q} \end{pmatrix} = \begin{pmatrix} \boldsymbol{\alpha}^{-1} - \boldsymbol{P} & -\boldsymbol{U} \\ \boldsymbol{R}\boldsymbol{U}^{\dagger} & \boldsymbol{T} \end{pmatrix}^{-1} \begin{pmatrix} \boldsymbol{E}^{\mathrm{QM+c}} \\ \boldsymbol{R}\boldsymbol{V}^{\mathrm{QM+c}} \end{pmatrix}. \tag{9}$$

The induced dipoles and PCM charges are therefore obtained simultaneously by solving, either iteratively or by matrix inversion, Eq. (9). The MM-PCM matrix is dimensioned $(N_{\mathrm{tes}} + 3N_{\mathrm{pol}}) \times (N_{\mathrm{tes}} + 3N_{\mathrm{pol}})$; matrix $\boldsymbol{U}$ is responsible for the MMPol/PCM mixing, and setting it to zero would decouple the problem.

2.2 The QM problem

Within the Born-Oppenheimer approximation, the QM solute satisfies the Schrödinger equation, where the Hamiltonian is divided into an unperturbed (gas-phase) term $\hat{H}^0$ and an perturbation term $\hat{H}^{\mathrm{env}}$ accounting for the coupling with the environment.

$$\hat{H}^{\mathrm{eff}} |\Psi\rangle = (\hat{H}^0 + \hat{H}^{\mathrm{env}}) |\Psi\rangle = E |\Psi\rangle . \tag{10}$$

The perturbation term includes all the energetic terms arising from the presence of a set of PCM charges and of a set of MMPol charges and induced dipoles. It can be expressed in terms of four contributions:

$$\hat{H}^{\mathrm{env}} = \hat{H}_{\mathrm{QM/PCM}} + \hat{H}_{\mathrm{QM/MM}} + \hat{H}_{\mathrm{MM/PCM}} + \hat{H}_{\mathrm{MM/MM}}, \tag{11}$$

where:

$$\hat{H}_{\mathrm{QM/PCM}} = \int d\boldsymbol{r} \sum_t \frac{\rho(\boldsymbol{r}) q_t^{\mathrm{PCM}}}{|\boldsymbol{r}-\boldsymbol{r}_t|} = \sum_t q_t^{\mathrm{PCM}} \hat{V}_t^{\mathrm{QM}}; \tag{12}$$

$$\begin{aligned}\hat{H}_{\mathrm{QM/MM}} &= \hat{H}^{\mathrm{el}}_{\mathrm{QM/MM}} + \hat{H}^{\mathrm{pol}}_{\mathrm{QM/MM}} \\ &= \int d\boldsymbol{r} \sum_c \frac{\rho(\boldsymbol{r}) q_c^{\mathrm{MM}}}{|\boldsymbol{r}-\boldsymbol{r}_c|} + \frac{1}{2} \int d\boldsymbol{r} \sum_p \rho(\boldsymbol{r}) \frac{\boldsymbol{\mu}_p(\boldsymbol{r}-\boldsymbol{r}_p)}{\left|\boldsymbol{r}-\boldsymbol{r}_p\right|^3} \\ &= \sum_c q_c^{\mathrm{MM}} \hat{V}_c^{\mathrm{QM}} - \frac{1}{2} \sum_p \boldsymbol{\mu}_p \hat{\boldsymbol{E}}_p^{\mathrm{QM}};\end{aligned} \tag{13}$$

$$\hat{H}_{\mathrm{MM/PCM}} = \sum_t \sum_c \frac{q_t^{\mathrm{PCM}} q_c^{\mathrm{MM}}}{|\boldsymbol{r}_t-\boldsymbol{r}_c|} = \sum_t q_t^{\mathrm{PCM}} \hat{V}_t^{\mathrm{MM}}; \tag{14}$$

$$\begin{aligned}\hat{H}_{\mathrm{MM/MM}} &= \hat{H}^{\mathrm{el}}_{\mathrm{MM/MM}} + \hat{H}^{\mathrm{pol}}_{\mathrm{MM/MM}} \\ &= \frac{1}{2} \sum_c \sum_{c' \neq c} \frac{q_c^{\mathrm{MM}} q_{c'}^{\mathrm{MM}}}{|\boldsymbol{r}_c-\boldsymbol{r}_{c'}|} + \frac{1}{2} \sum_c \sum_p q_c^{\mathrm{MM}} \frac{\boldsymbol{\mu}_p(\boldsymbol{r}_c-\boldsymbol{r}_p)}{\left|\boldsymbol{r}_c-\boldsymbol{r}_p\right|^3} \\ &= \frac{1}{2} \sum_c q_c^{\mathrm{MM}} \hat{V}_c^{\mathrm{MM}} - \frac{1}{2} \sum_p \boldsymbol{\mu}_p \hat{\boldsymbol{E}}_p^{\mathrm{MM}}.\end{aligned} \tag{15}$$

In the last equations, $\hat{V}$ and $\hat{\boldsymbol{E}}$ are the potential and electric field operators, respectively, due to the QM solute or to the MM charge distribution. For what concerns the latter terms, it is possible to consider the MM charges (constant both in position and size) as belonging to the set of "fixed charges" together with the nuclei. Therefore, the two MM electrostatic terms $\hat{H}^{\mathrm{el}}_{\mathrm{QM/MM}}$ and $\hat{H}^{\mathrm{el}}_{\mathrm{MM/MM}}$ can be included in a modified gas-phase Hamiltonian $\hat{H'}^0$, while the perturbation term can be written as:

$$\begin{aligned}\hat{H'}^{\mathrm{env}} &= \hat{H}_{\mathrm{QM/PCM}} + \hat{H}_{\mathrm{MM/PCM}} + \hat{H}^{\mathrm{pol}}_{\mathrm{QM/MM}} + \hat{H}^{\mathrm{pol}}_{\mathrm{MM/MM}} \\ &= \hat{H}_{\mathrm{QM+c/PCM}} + \hat{H}_{\mathrm{QM+c/MM}},\end{aligned} \tag{16}$$

where the label 'QM+c' indicates, as in Eq. (9), that the interaction is with the QM system (nuclei and electron density) plus the MM charges.

The Fock matrix contains extra 1-electron and 2-electron terms due to the environment (plus

the constant charge–charge interaction), so that it reads:

$$\boldsymbol{F} = \boldsymbol{h}^0 + \boldsymbol{G}^0(\boldsymbol{P}) + \boldsymbol{h}^{\mathrm{env}} + \boldsymbol{X}^{\mathrm{env}}(\boldsymbol{P}), \tag{17}$$

where $\boldsymbol{h}^0$ and $\boldsymbol{G}^0$ are the usual gas-phase 1- and 2-electron terms (plus the eventual contribution from the MM charges), while $\boldsymbol{h}^{\mathrm{env}}$ and $\boldsymbol{X}^{\mathrm{env}}$ arise from the interaction of the QM electron density with the PCM charges and MM charges and induced dipoles. In particular, the 1-electron term $\boldsymbol{h}^{\mathrm{env}}$ accounts for the interaction with both the PCM and the MM charges and the dipoles induced by the fixed charges (nuclei and MM charges), while $\boldsymbol{X}^{\mathrm{env}}$ accounts for the interaction with those induced by the electron distribution, i.e. those found by solving Eq. (9) with the electric field and potential due to the QM electronic wavefunction. These PCM charges and induced dipoles therefore depend themselves on the wavefunction, and this is stressed by explicitly indicating the term dependence on the density matrix $\boldsymbol{P}$.

2.3 TD-DFT and Electronic Energy Transfer

The QM/MMPol/PCM method has been implemented within the TD-DFT Linear Response scheme, in the same way it had been done for the PCM and MMPol independently. In a basis of single excitations between KS orbitals, solving Eq. (18) provides the excitation frequencies ω_n and the corresponding eigenstates $\begin{pmatrix} \boldsymbol{X}_n & \boldsymbol{Y}_n \end{pmatrix}^{\dagger}$:

$$\begin{pmatrix} \boldsymbol{A} & \boldsymbol{B} \\ \boldsymbol{B}^* & \boldsymbol{A}^* \end{pmatrix} \begin{pmatrix} \boldsymbol{X}_n \\ \boldsymbol{Y}_n \end{pmatrix} = \omega_n \begin{pmatrix} \mathbf{1} & \mathbf{0} \\ \mathbf{0} & -\mathbf{1} \end{pmatrix} \begin{pmatrix} \boldsymbol{X}_n \\ \boldsymbol{Y}_n \end{pmatrix}, \tag{18}$$

where $\boldsymbol{A}$ and $\boldsymbol{B}$ form the Hessian of the electronic energy. The inclusion of both PCM and MMPol effects in this picture is simply a combination of the two effects,[19,33,38] so that matrices $\boldsymbol{A}$ and $\boldsymbol{B}$

can be written as:

$$A_{ai,bj} = \delta_{a,b}\delta_{i,j}(\varepsilon_a - \varepsilon_i) + K^0_{ai,bj} + C^{\mathrm{PCM}}_{ai,bj} + D^{\mathrm{MMPol}}_{ai,bj} \tag{19}$$

$$B_{ai,bj} = K^0_{ai,jb} + C^{\mathrm{PCM}}_{ai,bj} + D^{\mathrm{MMPol}}_{ai,bj}, \tag{20}$$

where indices i and j label occupied orbitals and a and b virtual orbitals, and where matrices $\boldsymbol{K}$, $\boldsymbol{C}$ and $\boldsymbol{D}$ are written in terms of the orbitals as follows:

$$K_{ai,bj} = \int d\boldsymbol{r} d\boldsymbol{r}' \psi^*_a(\boldsymbol{r})\psi_i(\boldsymbol{r}) \left[\frac{1}{|\boldsymbol{r}-\boldsymbol{r}'|} + g_{\mathrm{xc}}(\boldsymbol{r},\boldsymbol{r}')\right] \psi^*_b(\boldsymbol{r}')\psi_j(\boldsymbol{r}'); \tag{21}$$

$$C^{\mathrm{PCM}}_{ai,bj} = \sum_t \left[\int d\boldsymbol{r} \psi^*_a(\boldsymbol{r})\psi_i(\boldsymbol{r}) \frac{1}{|\boldsymbol{r}_t - \boldsymbol{r}|}\right] q_t(\psi^*_b, \psi_j); \tag{22}$$

$$D^{\mathrm{MMPol}}_{ai,bj} = -\sum_p \left[\int d\boldsymbol{r} \psi^*_a(\boldsymbol{r})\psi_i(\boldsymbol{r}) \frac{\boldsymbol{r}_p - \boldsymbol{r}}{|\boldsymbol{r}_p - \boldsymbol{r}|^3}\right] \mu_p(\psi^*_b, \psi_j). \tag{23}$$

The term in Eq. (21), which is the only term present in vacuo, couples the $(i \to a)$ and $(j \to b)$ excitations through Coulomb and exchange-correlation kernels, while the PCM and MMPol terms of Eq. (22) and Eq. (23) may be interpreted as accounting for the Coulomb interaction between the $(i \to a)$ excitation and the solvent polarization response to the $(j \to b)$ excitation, i.e. an interaction mediated by the environment. Note that the PCM charges in Eq. (22) are obtained solving either Eq. (2) or Eq. (9), but using the optical permittivity of the solvent, ε_∞, i.e. only considering the fast solvent response. The MMPol induced dipoles are always considered as a fast response.

Eq. (18) can be generally written as $\boldsymbol{M}\boldsymbol{W}_n = \omega_n \boldsymbol{I}\boldsymbol{W}_n$; when the Linear Response treatment is generalised to a non-interacting couple of chromophores, sharing a resonance frequency ω_0, the equation can be written as:

$$\begin{pmatrix} \boldsymbol{M}_{\mathrm{DD}} & \boldsymbol{M}_{\mathrm{DA}} \\ \boldsymbol{M}_{\mathrm{AD}} & \boldsymbol{M}_{\mathrm{AA}} \end{pmatrix} \begin{pmatrix} \boldsymbol{W}_{\mathrm{D}} \\ \boldsymbol{W}_{\mathrm{A}} \end{pmatrix} = \omega \begin{pmatrix} \boldsymbol{I} & \boldsymbol{S}_{\mathrm{DA}} \\ \boldsymbol{S}_{\mathrm{AD}} & \boldsymbol{I} \end{pmatrix} \begin{pmatrix} \boldsymbol{W}_{\mathrm{D}} \\ \boldsymbol{W}_{\mathrm{A}} \end{pmatrix}, \tag{24}$$

where the indices D and A refer to the donor and acceptor, and $\boldsymbol{S}$ includes the overlap between

donor and acceptor orbitals. When the D/A interaction is turned on, the energies are no longer degenerate, and the electronic coupling between donor and acceptor is defined as half the resulting energy splitting. If the interaction is treated as a perturbation, Eq. (24) can be solved approximately and the coupling can be obtained from the first-order perturbed energies as:[15]

$$\begin{aligned} V &\equiv \frac{\omega_+ - \omega_-}{2} = \boldsymbol{W}_{\mathrm{D}}^{\dagger}\boldsymbol{M}_{\mathrm{DA}}\boldsymbol{W}_{\mathrm{A}} - \omega_0 \boldsymbol{W}_{\mathrm{D}}^{\dagger}\boldsymbol{S}_{\mathrm{DA}}\boldsymbol{W}_{\mathrm{A}} \\ &= \boldsymbol{W}_{\mathrm{D}}^{\dagger}\left(\boldsymbol{K}_{\mathrm{DA}} + \boldsymbol{C}_{\mathrm{DA}}^{\mathrm{PCM}} + \boldsymbol{D}_{\mathrm{DA}}^{\mathrm{MMPol}}\right)\boldsymbol{W}_{\mathrm{A}} - \omega_0 \boldsymbol{W}_{\mathrm{D}}^{\dagger}\boldsymbol{S}_{\mathrm{DA}}\boldsymbol{W}_{\mathrm{A}}. \end{aligned} \tag{25}$$

Note that matrices $\boldsymbol{K}_{\mathrm{DA}}$, $\boldsymbol{C}_{\mathrm{DA}}^{\mathrm{PCM}}$ and $\boldsymbol{K}_{\mathrm{DA}}^{\mathrm{MMPol}}$ differ from those of Eq. (21) — Eq. (23) in that the orbitals labelled i and a belong to the donor, while those labelled j and b belong to the acceptor; the same holds for the overlap matrix $\boldsymbol{S}_{\mathrm{DA}}$. When these matrices are contracted with $\boldsymbol{W}_{\mathrm{D}}^{\dagger}$ and $\boldsymbol{W}_{\mathrm{A}}$, the resulting contributions to the first-order coupling can be written in terms of the diagonal elements of the one-particle transition density matrices ("transition densities"), $\tilde{\rho}_{\mathrm{D}}$ and $\tilde{\rho}_{\mathrm{A}}$:

$$\begin{aligned} V_{\mathrm{Coul}} &= \int d\boldsymbol{r} d\boldsymbol{r}' \tilde{\rho}_{\mathrm{A}}^{\dagger}(\boldsymbol{r}) \frac{1}{|\boldsymbol{r}-\boldsymbol{r}'|} \tilde{\rho}_{\mathrm{D}}(\boldsymbol{r}'); \\ V_{\mathrm{xc}} &= \int d\boldsymbol{r} d\boldsymbol{r}' \tilde{\rho}_{\mathrm{A}}^{\dagger}(\boldsymbol{r}) g_{\mathrm{xc}}(\boldsymbol{r},\boldsymbol{r}') \tilde{\rho}_{\mathrm{D}}(\boldsymbol{r}'); \\ V_{\mathrm{Ovlp}} &= -\omega_0 \int d\boldsymbol{r} \tilde{\rho}_{\mathrm{A}}^{\dagger}(\boldsymbol{r}) \tilde{\rho}_{\mathrm{D}}(\boldsymbol{r}); \\ V_{\mathrm{PCM}} &= \sum_t \left[\int d\boldsymbol{r} \tilde{\rho}_{\mathrm{A}}^{\dagger}(\boldsymbol{r}) \frac{1}{|\boldsymbol{r}-\boldsymbol{r}_t|} \right] q_t(\tilde{\rho}_{\mathrm{D}}); \\ V_{\mathrm{MMPol}} &= -\sum_p \left[\int d\boldsymbol{r} \tilde{\rho}_{\mathrm{A}}^{\dagger}(\boldsymbol{r}) \frac{\boldsymbol{r}_p - \boldsymbol{r}}{|\boldsymbol{r}_p - \boldsymbol{r}|^3} \right] \mu_p(\tilde{\rho}_{\mathrm{D}}). \end{aligned} \tag{26}$$

The definitions reported in Eq. (26) show that the first-order electronic coupling between two chromophores can be calculated from the transition densities of the non-interacting chromophores. In practice, a coupling calculation is performed in two stages: first the transition densities of the isolated chromophores are calculated ('monomer stage'); then, these are combined to obtain the coupling ('coupling stage'). The first three terms of Eq. (26) are present in vacuo; the exchange-correlation and overlap terms are often negligible, compared to the Coulomb term. The PCM

and MMPol terms describe the interaction between the acceptor transition density with the PCM charges and MMPol dipoles induced by the donor one.

3 Computational details

All the QM calculations were run at the TD-DFT level, employing the CAM-B3LYP functional[39] and the 6-31G(d) basis set, using a locally modified version of the Gaussian09 suite of codes.[40] The choice of the functional and the basis set was done mainly to maintain the consistency with previous studies on the same systems.

As for MMPol parameters, the fixed MM charges were obtained from a fit of the electrostatic potential of the molecule or fragment, using the Merz and Kollman method.[41,42] The CAM-B3LYP functional and 6-31G(d) basis set were used in the calculations, consistently with the QM calculations. The problem eventually arising from the presence of covalent bonds between the QM and the MM fragments was tackled by following the link atom method:[43] the QM-MM bonds were initially cut and saturated on both sides with hydrogens. The saturated MM fragment, isolated, was then used to obtain the Merz-Kollman (MK) charges; afterwards, the MM atoms previously bound to the QM chromophores, together with their saturation hydrogens, were removed to avoid hyperpolarization problems; their MM charges were summed and distributed onto the covalently bound MM atoms.

The polarizable sites coincide with the MM atoms. The values of the isotropic polarizabilities placed on each atom depend on the MM treatment of polarization chosen. We adopted the Thole model, which avoids intramolecular overpolarization problems by using a smeared dipole-dipole interaction tensor.[44] Atomic isotropic polarizability values were taken from the fit of experimental molecular polarizabilities performed by van Duijnen and Swart using the linear version of Thole dipole-dipole tensor.[45] We also tested the polarizabilities derived recently in the context of the Amber force field,[46] always finding little dependence of the results on the model used.

The continuum solvent description was based on the IEF formulation of the PCM model,[35,36]

using the discretization procedure into point charges available in Gaussian09 asking for the Gaussian03 defaults.

In order to obtain representative structures of the distribution of toluene solvent molecules around the PDI-TDI system, we also performed classical molecular dynamics simulations of the dyad, in which the structure of the PDI-TDI molecule was kept frozen. The simulation system was built by solvating the dyad in a toluene box (buffer zone of 20 Å) using the Leap module of the Amber9 suite of programs.[47] Both the toluene solvent and the PDI-TDI dyad were described using the GAFF force field.[48] The system was initially thermalized by running a 100-ps MD simulation at constant volume in order to increase the temperature from 100 K to 298 K. Then, a 100-ps equilibration at constant pressure (1 atm) and temperature (298 K) was performed using standard coupling schemes in order to reach an appropiate density of the toluene solution. Finally, the simulation was extended for 2 ns for production purposes. All runs were performed with Amber9 using an integration time step of 1 fs, periodic boundary conditions, the Particle Mesh Ewald approach to deal with long-range electrostatics, and a nonbonded cutoff equal to 10 Å. For pressure regulation, an isothermal compressibility of 92 TPa^{-1} was used for toluene.

4 Results

There are various instances when a coupled fully-polarizable QM/MM/PCM model is desirable. We present and discuss here the study of two different cases.

The first case presented in Section 4.1 considers Donor–Bridge–Acceptor (DBA) systems in which the donor and acceptor chromophores are treated quantum mechanically, the bridge is described at MMPol level and the solvent is introduced as a polarizable continuum. The advantages and limitations of such a mixed QM/classical description of the solute are discussed.

The second case where QM/MM/PCM is applied, in Section 4.2, considers instead a full-QM solute surrounded by a solvent. The first solvation shell, comprising solvent molecules within a certain distance (cutoff) to the solute, are described at MMPol level to exploit the structural

information extracted from a molecular dynamics simulation (MD); PCM is used for the rest of the solvent, beyond the cutoff distance.

4.1 MMPol description of the bridge in DBA systems

As described in the Introduction, in DBA systems the bridge may affect the excitation energy transfer rates between the donor and the acceptor via two mechanisms: superexchange and mediated Coulomb interaction. The first is a long-range through-bond mediated exchange interaction involving the orbitals of the bridge; it resembles the electron transfer exchange interaction and is quantum-mechanical in character. The mediated Coulomb interaction, on the other hand, is electrostatic in character and depends on the polarizability of the bridge. It has been observed that such interaction may either increase or reduce the donor/acceptor coupling (see for instance Fückel et al.[28] and Chen et al.[30]), and that the bridge effect is in general a complex phenomenon dependent on the bridge orientation, and possibly characterized by anisotropic polarizabilities.[12]

For this reason, if one wants to carry out a mixed study on DBA systems, where the chromophores are described at a QM level and the bridge at a lower level, a model retaining structural information of the bridge and accounting for its anisotropic polarizability should be employed, rather than averaged models. At the same time, full-QM models, where both the chromophores and the bridge are treated quantum-mechanically, may be cumbersome and computationally expensive. The polarizable MMPol model[19] seems to be an ideal compromise, as it greatly reduces the computational requirements of a full QM description, but at the same time correctly describes the bridge charge distribution and polarizability. The first aim of this section is to investigate whether such a classical polarizable description of the bridge correctly reproduces the enhancement of the D/A coupling which has been observed in some DBA systems, and which has been ascribed to mediated Coulomb interactions. At the same time, we expect our model to fail whenever the bridge effect is quantum-mechanical in character (e.g. in case of a superexchange effect).

Two families of DBA systems, characterized by a significant effect of the bridge on the electronic coupling, have been studied. The systems have been selected so to allow a direct comparison

with the "exact" benchmark, e.g. a full QM description. The general approach followed here consists in comparing the coupling results obtained when the bridge is treated quantum-mechanically to those obtained when it is treated classically, with the MMPol model. The solvent is then considered as a PCM charge distribution, placed on the molecular cavity.

4.1.1 PDI-TDI and PMI-TDI systems

Previous studies on electronic energy transfer in a perylene diimide – terrylene diimide (PDI-TDI) dyad, separated by a substituted terphenyl spacer (see Figure 1), have shown a strong deviation from Förster behavior.[49]

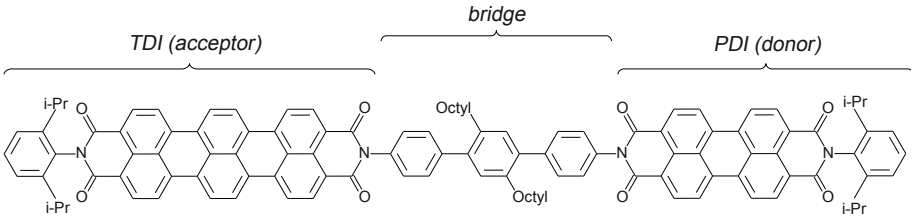

Figure 1: Structure of the PDI-TDI dyad investigated in this work.

The dyad is characterized by a weak electronic coupling; a QM study by Curutchet et al.[27] has shown that the bridge does not affect the donor and acceptor transition energies, but it strongly enhances the coupling by 56%, and also induces a slight delocalization of the donor and acceptor transition densities over the bridge. The procedure followed in that study consisted in building several systems comprising the chromophores and the three phenyl units, variously arranged. The simplest of these models included no bridge at all, while the more complete ones included all three phenyl units, differently arranged. The bridge phenyl units were always treated at a QM level, either as part of the donor or the acceptor.

In the present study, we follow a similar procedure, defining four different QM models (M0, M1, M2 and Mc) and one MMPol model (labelled MMPol). Model M0 includes the two chromophores only, and no bridge; model M1 (model M2) includes one (two) of the bridge phenyl units (see Figure 1), whereas Mc includes all the bridge phenyl units. We note that M1, M2 and Mc models can be obtained in different ways; for example for M1 there are two possible configu-

rations, one with the phenyl unit bound to the acceptor and the other with the same unit bound to the donor. The number of alternative configurations increases for M2, which can be realized with three alternative configurations, and for Mc, for which the configurations are four ($PDIPh_3$/TDI and the complementary one but also $PDIPh_2$/TDPh and the complementary one). However, as demonstrated by Curutchet et al.,[27] the coupling depends much more strongly on the number of phenyl units included in the picture, rather than on how these are arranged. In all the cases here tested, the coupling differences between two configurations of the same model are always below 4%. The electronic coupling results we present in this section are therefore averaged over all the possible different configurations for each model.

In the model labelled MMPol, a mixed QM/MM description of the DBA system is employed: the chromophores are described at QM level, while the whole bridge (the three phenyl units) are described as a classical polarizable distribution of point charges and induced dipoles, according to the MMPol scheme. This model is clearly able to include eventual polarization effects of the bridge, while disregarding all QM effects, and may therefore provide useful information on the role of the bridge itself in the EET process.

For each model, two sets of calculations are run: one in vacuo and one in toluene; in the latter case, the solvent is described at PCM level.

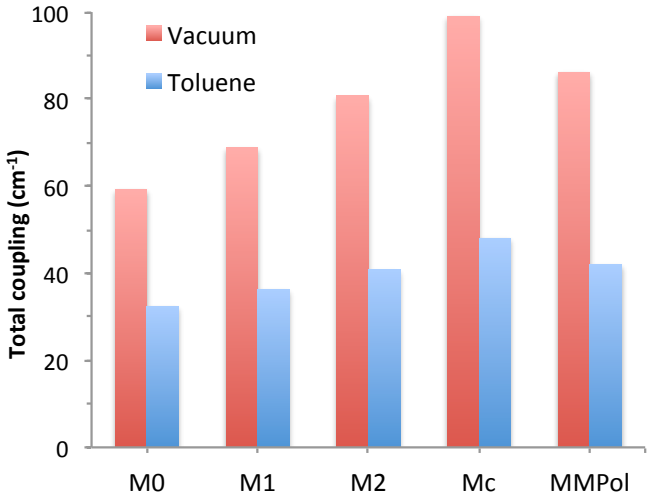

Figure 2: Total coupling (cm^{-1}) of the PDI-TDI dyad. Models M0, M1, M2, Mc and MMPol: see text. Red bars: coupling in vacuo; blue bars: coupling in toluene, described through PCM.

The couplings obtained are reported in Table 1 (exchange-correlation and overlap terms are not reported as they are negligible). The total couplings are shown in Figure 2. Red bars refer to calculations in vacuo, blue ones to those in toluene.

Comparing the QM models, M0 through Mc, we notice the strong coupling enhancement due to the presence of the bridge between the chromophores; such effect is estimated in Table 1 as the percentage difference between the total coupling of each model and that of M0. Including the full bridge results in a 67% and 48% increase of the coupling in vacuo and in toluene, respectively, in agreement with the previous studies.[27]

The MMPol model should be compared to the Mc one, as they both include the whole bridge, although at different levels (QM and MMPol, respectively). From Table 1 we observe that the Coulomb coupling term in the MMPol model is similar to that in the M0 model, which is reasonable, while the enhancement effect of the bridge is accounted for in the explicit MMPol coupling term, V_{MMPol}. Comparing the total coupling from Mc and MMPol models, we observe that such enhancement effect is roughly reproduced, although it is somehow underestimated by the MMPol model, with errors around 13% both in vacuo and in toluene.

Assuming that the contributions to the coupling arise from both through-space polarization effects and through-bond QM effects, and considering that the latter are completely disregarded by the classical MMPol model, we can interpret the discrepancies observed between the two models and estimate the through-space polarization effect of the bridge to be approximately ranging from 68% to 60% of the total coupling (as obtained from results in vacuo and in toluene, respectively).

Table 1: Electronic coupling (in cm^{-1}) for the PDI-TDI dyad in toluene, arranged according to various models (see text). (a): Estimate of the bridge contribution as the percentage difference with M0 total coupling. (b): The values reported are the average over the different configurations within the same model.

	Vacuum				Toluene				
Model	V_{Coul}	V_{MMPol}	V_{TOT}	B.C.[a]	V_{Coul}	V_{MMPol}	V_{PCM}	V_{TOT}	B.C.[a]
M0	59.3	—	59.3		75.1	—	−42.6	32.5	
M1[b]	68.8	—	68.8	(16%)	84.1	—	−47.8	36.4	(12%)
M2[b]	80.7	—	80.7	(36%)	93.7	—	−52.9	40.8	(26%)
Mc[b]	99.1	—	99.1	(67%)	106.1	—	−57.9	48.1	(48%)
MMPol	61.5	24.7	86.2	(46%)	76.4	17.5	−51.8	42.0	(29%)

As pointed out in previous studies, the presence of the bridge does not significantly affect the character of the electronic excitations in the chromophores. As an example, in Figure 3 we show the HOMO and LUMO molecular orbitals of the donor molecule, whose $S_0 \rightarrow S_1$ excitation is dominated by the HOMO $\rightarrow$ LUMO transition, for both the M0 and the Mc models. When the whole bridge is considered as part of the donor molecule (Mc model), the excitation is still dominated by the same transition and the HOMO and LUMO do not seem to be significantly distorted with respect to the M0 case (plots (a) and (b)), although the transition density shown in plot (c) shows small contributions on the bridge atoms. Such a small delocalization of the transition density over the bridge, already observed by Curutchet et al.,[27] can be mediated by wavefunction overlap, and thus may explain the disagreement between Mc and MMPol couplings observed in Figure 2.

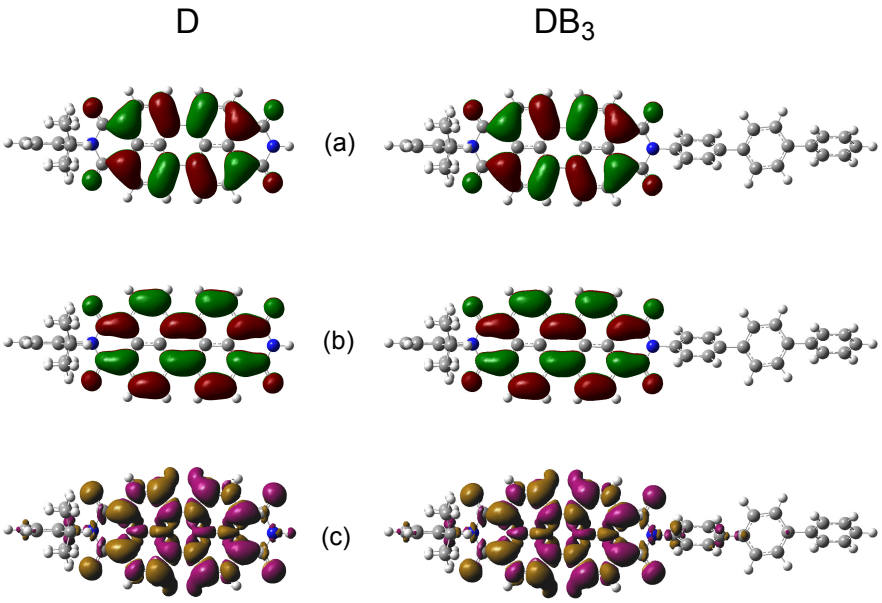

Figure 3: HOMO (a) and LUMO (b) molecular orbitals, and ground to first excited state transition density (c) of the isolated PDI (D) and the PDI-Bridge configuration (DB_3). Surface isovalue 0.01 a.u. in (a) and (b), 0.002 a.u. in (c).

When the solvent is included in the picture, the resulting total coupling values (plotted as blue bars in Figure 2) show an evident decrease due to the overall screening effect of the solvent, which reduces the total coupling to up to 50% of the value in vacuo. In particular, see also the explicit PCM term, V_{PCM}, in Table 1, arising from the interaction of the donor transition density with the

solvent polarization charges induced by the acceptor transition density (see Eq. (26)). The implicit solvent effect on the Coulomb term, on the other hand, is positive (compare V_{Coul} in vacuo and in toluene).

Conversely, the presence of the PCM solvent induces a decrease of the explicit MMPol term, V_{MMPol}, which is reduced from 24.7 to 17.5 cm^{-1}. This effect is caused by the solvent reaction field opposing the field generated by the QM chromophores, and thus reducing the effective field on the MMPol atoms and consequently their polarization.

The results on the PDI-TDI system show that most of the bridge effect can be reproduced by a classical model; as a comparison, we performed a similar set of calculations on a related DBA system, a perylene monoimide – terrilene diimide dyad with a ladder-type pentaphenylene – phenylene bridge (PMI−pPh−Ph−TDI, shown in Figure 4). Contrary to the PDI-TDI, in this case the bridge is strongly coupled to the donor unit, so that the optical spectra of the PMI-pPh molecule change significantly with respect to those of the bare PMI.[31] In this case, the PMI−pPh excitation shows a strong charge-transfer character, so a purely electrostatic description of the D-B coupling provided by the MMPol model is expected to break down.

To verify this prediction we have repeated the same analysis previously applied to PDI-TDI dyad and we have compared different QM models including no bridge (M0 = PMI / TDI), the –Ph unit (M1 = PMI / TDI-Ph), the –pPh unit (M2 = PMI-pPH / TDI) and the complete Ph-pPh bridge (Mc = PMI-pPH / TDI-Ph). The whole bridge is also included in the MMPol model but in a fully classical way. For each model, two sets of calculations are run: one in vacuo and one in toluene; in the latter case, the solvent is described at the PCM level.

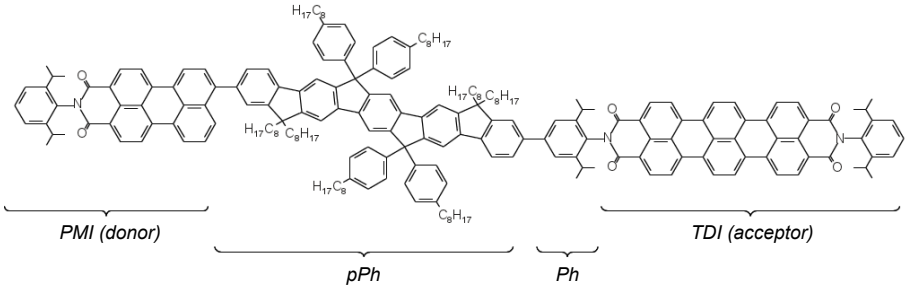

Figure 4: Geometry of the PMI-TDI dyad.

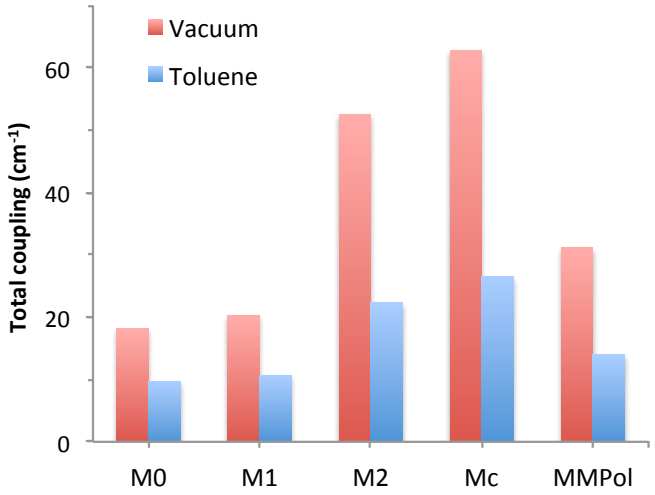

Figure 5: Total coupling (cm^{-1}) of the PMI-TDI dyad. Models M0, M1, M2, Mc and MMPol: see text. Red bars: coupling in vacuo; blue bars: coupling in toluene.

As Figure 5 shows, the coupling enhancement effect induced by the pPh spacer is very large, but it is almost completely lost in MMPol calculations, as expected. The results do not qualitatively change when we include the solvent (toluene) but what we see is just a reduction of the coupling due to the explicit PCM term.

4.1.2 ZnFbB(CH_3)$_4$ system

Another system studied is a porphyrin dimer. Several studies showed that dimers of Zinc (Zn) and metal-free (Fb) porphyrins, linked by semirigid bridges, have interesting properties; in particular, some are characterized by a rapid and highly efficient energy transfer from the Zn-porphyrin (donor) to the metal-free one (acceptor).[50–52] We present here the results on one of these dimers, having a diaryl-ethyne linker, referred to as ZnFbB(CH_3)$_4$ in the paper by Strachan et al.;[52] its structure is shown in Figure 6.

In order to assess the influence of the bridge on the coupling, and whether a classical description is appropriate for it, we have built four models following what did before for the other two systems. As before, model M0 completely neglects the bridge whereas Mc includes the entire bridge at QM level. We note that, in Mc, the partition into donor and acceptor can be done either associating the

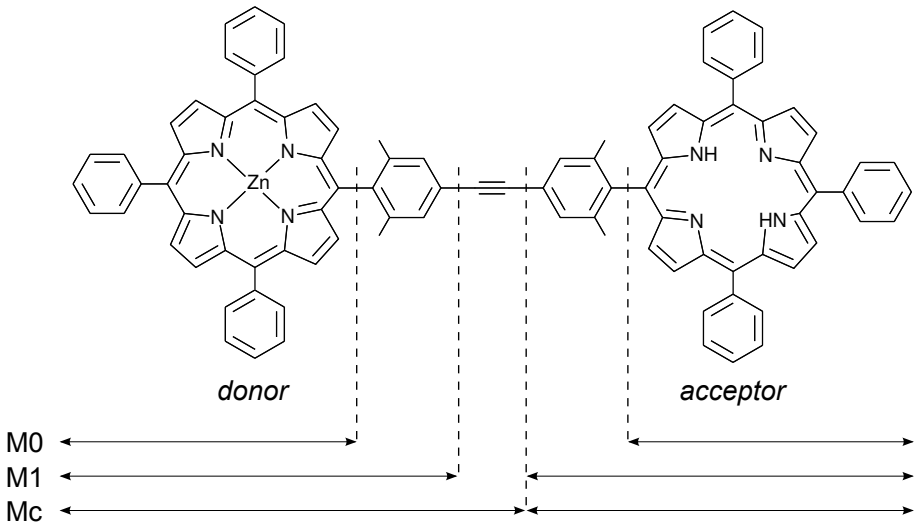

Figure 6: Structure of the $ZnFbB(CH_3)_4$ dimer investigated in this work.

phenyl-ethyne unit to the Zn-porphyrin or the way around: here we report data only for first choice as the results do not change in the other case. In addition, an intermediate M1 model is defined in which only the two phenyl groups of the bridge are considered as parts of the QM chromophores whereas the ethyne is neglected. Finally, in the model labelled MMPol the QM chromophores are as in M0, but the whole bridge is included at the MMPol level.

Table 2 reports the excitation energies obtained in vacuo for the four models.

Table 2: Excitation energies, in eV, relative to the first four states of the donor and acceptor chromophores of $ZnFbB(CH_3)_4$ dimer, in the four models considered.

	Acceptor				Donor			
Model	S_1	S_2	S_3	S_4	S_1	S_2	S_3	S_4
M0	2.14	2.36	3.45	3.54	2.35	2.35	3.54	3.57
M1	2.12	2.33	3.40	3.49	2.33	2.33	3.50	3.50
Mc	2.12	2.33	3.40	3.49	2.33	2.33	3.50	3.50
MMPol	2.14	2.35	3.42	3.52	2.35	2.35	3.53	3.53

Note the quasi-degeneration of states 1 and 2 and of states 3 and 4; this is more evident for the donor chromophore, containing the Zn atom, because of the D_4 symmetry, which is broken in the metal-free porphyrin. Moreover, the results indicate that the effects of including the bridge are very small (the changes from M0 to Mc are less than 1% for all states) and the MMPol description correctly reproduces all the states with the respective quasi-degeneracies.

For what concerns the coupling results, we present in Table 3 the couplings between all possi-

ble pairs of the bright states reported in Table 2 (the third and fourth excited states). The oscillator strengths of these B-states are between 1.2 and 1.6, while those of the lower Q-states are approximately between 0.001 and 0.01.

Table 3: Electronic coupling terms in cm^{-1}, in vacuo, between the strong B-states of the ZnFb porphyrin dimer studied. $V_{i,j}$ indicates the electronic coupling between the donor's S_i state and the acceptor's S_j state.

		$V_{3,3}$			$V_{3,4}$	
Model	V_{Coul}	V_{MMPol}	V_{TOT}	V_{Coul}	V_{MMPol}	V_{TOT}
M0	59.1	—	59.1	48.8	—	48.8
M1	48.6	—	48.6	48.2	—	48.2
Mc	157.1	—	156.4	195.9	—	194.7
MMPol	86.0	46.3	132.3	88.1	50.9	139.1
		$V_{4,3}$			$V_{4,4}$	
Model	V_{Coul}	V_{MMPol}	V_{TOT}	V_{Coul}	V_{MMPol}	V_{TOT}
M0	62.5	—	62.5	85.7	—	85.7
M1	125.2	—	125.2	148.6	—	148.6
Mc	58.7	—	58.6	34.1	—	34.2
MMPol	53.5	-9.4	44.1	58.3	-8.8	49.4

For models Mx, the only important contribution to the coupling comes from the Coulomb interaction, since exchange-correlation and overlap contributions (not reported) are negligible. In order to compare the different models one has to take into account that shifts between the (quasi) degenerate states are possible moving from one model to the other. In particular, from the analysis of the data reported in Table 3 it is evident that introducing the full bridge induces a shift between the states 3 and 4 in the donor. As a result $V_{3,i}$ of Mc corresponds to $V_{4,i}$ of M0 and M1 and viceversa: this shift is exactly reproduced by the MMPol description.

To have a more direct analysis, in Figure 7 we report a graph of the total couplings obtained as a sum of all the couplings listed in Table 3. Both results in vacuo and in toluene are shown.

We first analyze the vacuum results. Moving from M0 to Mc (i.e. including the bridge in the picture) the coupling increases by 42%. Similarly, in MMPol model such enhancement is provided by the MMPol coupling term, V_{MMPol}, which explicitly accounts for the polarization effect of the bridge: the Mc and MMPol difference is ca. 17%.

When introducing a continuum description of the solvent (toluene), we observe a reduction of the total coupling, because of the explicit PCM term which opposes the Coulomb coupling.

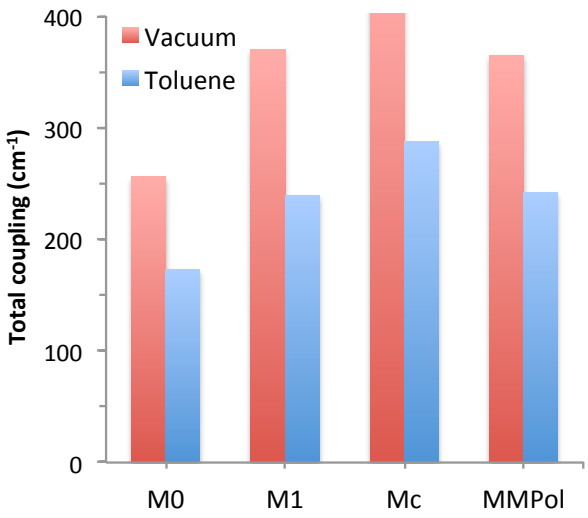

Figure 7: Total coupling (cm^{-1}) in the $ZnFb(CH_3)_4$ dyad. Models M0, M1, Mc and MMPol: see text. Red bars: coupling in vacuo; blue bars: coupling in toluene.

Again, moving from M0 to Mc results in a marked increase (40%) of the coupling; this is again reproduced by the MMPol model, where the explicit MMPol term favors the Coulomb coupling against the PCM term: the Mc and MMPol difference is ca. 16%, i.e. similarly to what found for the PDI-TDI dyad.

From the results obtained for the PDI-TDI dyad and $ZnFbB(CH_3)_4$, we can conclude that employing a classical polarizable description of the bridge, in DBA systems where there is no QM mixing between chromophore and bridge orbitals, provides a reliable and quick alternative to the full-QM treatment, and can be successfully coupled to an average polarizable description of the solvent through a PCM description.

To complete the analysis, it is important to explore another applicability of the QM/MMPol/PCM model, related to the description of the solvent effects. To this scope, we have compared three different formulations to describe the solvent, namely a full continuum (PCM) decription, a full atomistic (MMPol) description, and a mixed (MMPol/PCM) description: atomistic for the first solvation shells, and continuum for the rest of the solvent. This final analysis is here performed on the PDI-TDI dyad when immersed in toluene.

4.2 Description of the solvent

Discrete and continuum models follow almost opposite approaches in describing the effect of the solvent on QM solutes, and they may be thought as complementary for what concerns their advantages and disadvantages. Discrete QM/MM models have the advantage of retaining information on the solvent structure, and therefore of being able to describe short-range, specific solute–solvent interactions with good accuracy. At the same time, in order to get a correct picture of the dynamic solute–solvent interaction, it is necessary to sample a large number of configurations from a molecular dynamics simulation. Conversely, continuum solvation models describe the solvent in an averaged way, and therefore do not need configuration sampling. However, the solvent structural information is lost, and specific solute–solvent interactions are neglected.

The idea beyond a mixed discrete/continuum modeling of the solvent is then to try and combine the two models in order to exploit their complementary strengths: a discrete representation of the solvent molecules at short range may correctly describe the specific interactions, even using a relatively small number of configurations. For what concerns the average, long-range interactions, a continuum model may be employed beyond the discrete shell of solvation.

With this in mind, we have carried out a study to verify the advantages of such mixed approach in the calculation of the chromophore properties and electronic coupling of the PDI-TDI dyad in toluene. First, we ran a classical MD simulation of the system and extracted 11 structures from the trajectory. For each structure, several cutoff radii were applied, so that toluene molecules located further than the cutoff from the closest QM atom were discarded. Cutoff values of 0 (with no explicit solvent molecules), 3, 5, 8, 10, 15 and 30 Å were used. The average number of solvent molecules, $\langle n_{\mathrm{solv}} \rangle$, included in each case is reported in Table 4.

For each configuration, at each cutoff value, two coupling calculations are run, both describing the PDI-TDI dyad at QM level (using the previous Mc model) and the explicit solvent molecules at MMPol level. In one set, however, an extra PCM layer is considered to account for the long-range solvent effect beyond the cutoff. We will refer to this set as QM/MMPol/PCM, while the set that does not include the continuum solvent description on top of the discrete one will be referred to as

Table 4: Average dimensions of QM/MMPol and QM/MMPol/PCM calculations. (a) The matrix dimension is $(N_{\mathrm{tes}}+3N_{\mathrm{pol}})^2$; (b) for cutoff 8 Å the cavity is discretised into larger tesserae to reduce the computational demand; (c) no QM/MMPol/PCM calculations run for cutoffs larger than 8 Å.

Cutoff					Dimension / 10^6 (a)	
/ Å	$\langle n_{\mathrm{solv}}\rangle$	$\langle N_{\mathrm{tes}}\rangle$		$\langle 3N_{\mathrm{pol}}\rangle$	QM/MMPol	QM/MMPol/PCM
0.0	0	3564		0	0	13
3.0	50	14075		2235	5	266
5.0	73	17406		3276	11	428
8.0	169	20265	(b)	7605	58	777
10.0	235	—	(c)	10590	112	—
15.0	428	—	(c)	19272	371	—
30.0	558	—	(c)	25110	630	—

QM/MMPol.

Before presenting the results, we recall that the computational complexity of the inclusion of the environment effects can be roughly estimated considering the dimension of the MMPol, PCM or MMpol/PCM matrices, depending respectively on $(3N_{\mathrm{pol}})^2$, $(N_{\mathrm{tes}})^2$ and $(N_{\mathrm{tes}}+3N_{\mathrm{pol}})^2$, where N_{tes} is the number of tesserae forming the molecular cavity and N_{pol} the number of polarizable sites (in our case, the number of MM atoms). The average number of tesserae and polarizable sites and the average dimension of the matrices are reported in (Table 4) for the different choices of the cutoffs.

It is evident that each single QM/MMPol/PCM calculation is generally much more computationally expensive than each QM/MMPol one. However, the data reported in (Table 4) does not include any possible optimization of the PCM description when combined to the MMPol. As a matter of fact, it is reasonable to assume that when the first solvation shells are treated explicitly, the additional PCM description can be treated with lower numerical accuracy than the case where a pure PCM description is used. In particular, the quality of the mesh used can be significantly reduced with a corresponding important reduction of N_{tes}. This and other numerical aspects of the implementation have not been investigated in this paper but surely need to be optimized to obtain the required efficiency: efforts in this direction are in progress.

Figure 8 shows the excitation energy of the chromophores (top: acceptor, bottom: donor) as a function of the cutoff. The blue line represents the values obtained from a QM/MMPol picture,

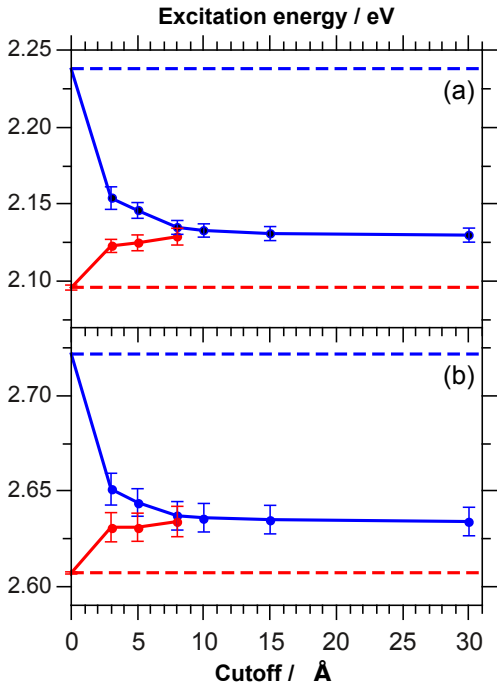

Figure 8: Excitation energies (eV) of the PDI-TDI chromophores (top: acceptor, bottom: donor) as a function of the cutoff. The blue and the red line represent the values obtained from a QM/MMPol and a QM/MMPol/PCM description, respectively.

where the QM solute is solvated by an increasing number of explicit solvent molecules at MMPol level. Note that at cutoff 0 the calculation is a pure QM in vacuo (the relative value is shown as a horizontal blue line). While more toluene molecules are included in the picture, the excitation energy decreases from $\sim$ 2.23 and converges to $\sim$ 2.13 eV, for the acceptor, while it starts from $\sim$ 2.72 and converges to $\sim$ 2.63 eV, for the donor. The inclusion of discrete molecules therefore lowers the excitation energy of $\sim$ 0.1 eV in both cases.

The red line of Figure 8, similarly, shows the excitation energy obtained from QM/MMPol/PCM calculations, where the QM solute and discrete solvent molecules are enclosed in a PCM cavity that simulates the long-range solvent response beyond the cutoff. The value at cutoff 0, where no explicit solvent molecule is included, corresponds to the pure PCM calculation, and is indicated by a horizontal red line. The QM/MM/PCM results clearly tend to the same value to which the QM/MMPol result tend ($\sim$ 2.13 and 2.63 eV for the acceptor and donor respectively); the calculations are run up to a cutoff value of 8 Å.

Before analyzing the figure, we note that the values reported on this plots and on the following ones refer to the average value from the 11 snapshots considered which have been proven to be sufficient to represent averaged values for such a low interacting solvent as toluene. The error bars show the standard deviation σ.

The observation of the different behavior shown by the blue and red lines in the figure provides information on the different solvation approaches used. The first observation concerns the pure-QM and pure-PCM values. If we take the value obtained at a cutoff of 30 Å as the reference value, we firstly observe that the effect of the solvent is to lower the energy by $\sim$ 0.1 eV with respect to isolated molecule, as noted before. The pure-PCM calculation provides an excitation energy in very good agreement to the reference value but the solvent effect is somehow overestimated.

A second remark concerns the convergence speed. Both QM/MMPol and QM/MMPol/PCM calculations tend to the same limit when the cutoff is increased, but the latter model, starting from a closer value to the reference, seems much quicker in converging, and provides a very accurate value (error $\sim$ 0.3%) already at cutoff = 3 Å. The QM/MMPol model, on the other hand, converges more slowly and provides results of comparable accuracy around a cutoff of 8 Å.

Similar conclusions can be drawn from the observation of Figure 9, where the transition dipole moment relative to the $S_0 \rightarrow S_1$ transition is shown for both the acceptor (top) and donor (bottom) molecules. Again, as expected, the simple inclusion of a continuum solvent, with no explicit MM molecules, provides results in good agreement to the limit value, although the effect of the solvent is overestimated. Again, note the quicker convergence of the QM/MM/PCM model. Finally, we note a small discontinuity in the convergence behavior of QM/MM/PCM results moving from 5 to 8 Å. This could be due to different settings in the tessellation of the PCM cavity: for cutoff 8 Å a larger average area of the tesserae has been set, in order to reduce the number of tesserae and the computational complexity. Such discontinuity is however negligible if compared to the standard deviation of the sample.

Finally, in Figure 10, we present the results obtained for the electronic couplings. In all plots we observe the same general behavior pointed out before: at cutoff 0, pure-PCM results are close

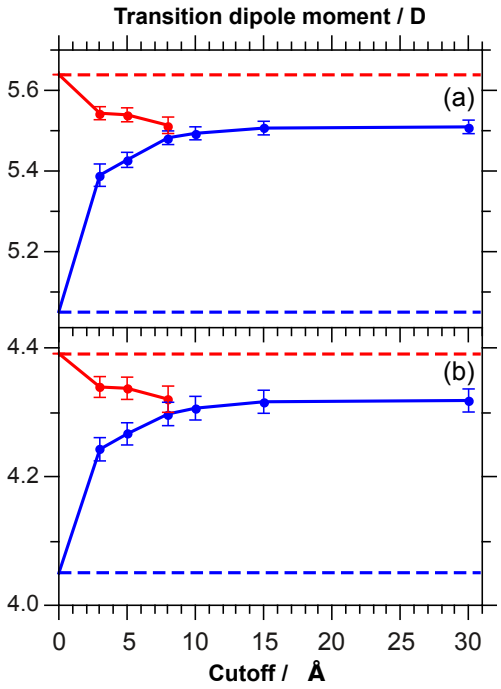

Figure 9: Transition dipole moments (Debye) of the PDI-TDI chromophores (top: acceptor, bottom: donor) as a function of the cutoff. The blue and the red line represent the values obtained from a QM/MMPol and a QM/MMPol/PCM description, respectively.

to the reference value (cutoff=30 Å), but slightly overestimating the solvent effects; QM/MM and QM/MM/PCM values tend to the same limit, but the latter converge more quickly. More in detail, it is evident from inspecting Figure 10(a) that the inclusion of long-range solvent effects through the PCM model greatly improves the estimate of the total coupling, even at very small cutoffs: the pure-PCM value underestimates the reference coupling by only 5 cm^{-1}, and the QM/MM/PCM model converges at 8 Å. It can be argued from this behavior that the main solvent effect to the total coupling is due to the average long-range polarization, well described at PCM level, while short-range specific effects do not amount to more than 5 cm^{-1}. This clearly depends on the nature of the solvent itself and we expect a different behavior when different solvents are modeled.

The explicit solvent effects are shown in Figure 10(b); the QM/MM/PCM results, displayed as a red line, contain both explicit solvent effects from the MM distribution and average effects from the PCM distribution. These effects are shown separately as a green and an orange line, respectively. The effect of the MMPol distribution in the QM/MM/PCM model (green line) is

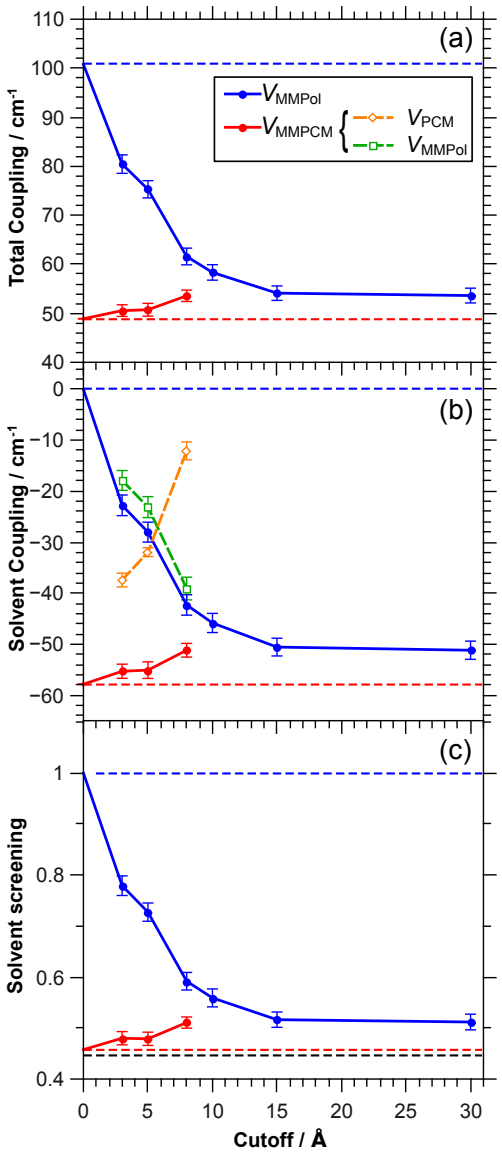

Figure 10: Electronic couplings (in cm^{-1}) vs. cutoff radius for the PDI-TDI dyad: Total V_{TOT} (a) and Solvent $V_{MMPol}[+V_{PCM}]$ (b) terms; solvent screening factor (c). Blue lines: QM/MM calculation; red lines: QM/MM/PCM calculation. Green and orange lines: MMPol and PCM individual contributions to the MMPCM coupling, respectively. The error bars ($\pm\sigma$) for the 11-configuration sample are shown.

very similar to the effect of the same distribution in the QM/MM model (blue line), while the effect of the PCM contribution (orange line) is, as expected, responsible for lowering the total MMPCM coupling closer to the reference limit. Moving to larger cutoff values, the PCM term increases almost by the same amount the MMPol term decreases, which results in the relatively small variation of the QM/MM/PCM coupling (red line) at different cutoffs.

Finally, Figure 10(c) reports the solvent screening factor, s, which can be thought, in a simple dipole–dipole picture, as the effective screening of the Coulomb interaction due to the solvent. It is defined as: $s = \frac{V_{\mathrm{TOT}}}{V_{\mathrm{Coul}}}$, so that $V_{\mathrm{TOT}} = sV_{\mathrm{Coul}}$. In Förster theory, s is calculated as the inverse of the solvent refractive index squared, but other approximations exist, based on different assumptions. The Förster screening factor is indicated in Figure 10(c) as a horizontal black line, and is in good agreement with our pure-PCM result (horizontal red line), around 0.45. The limit of the QM/MM and QM/MM/PCM calculations is also close, at around 0.5. This confirms our previous conclusion, that the solvent effect is mostly an average, long-range effect, which is well reproduced by a pure PCM model.[22]

5 Conclusions

We have presented the formulation, the computational implementation and some applications of a fully polarizable QM/MM/PCM approach to describe EET processes in (supra)molecular systems in condensed phase. The model allowed us to assess the possibility to describe solvent (screening) and bridge-mediated contributions to EET in solvated bridged bichromophoric systems based on a classical polarizable description of the solvent and bridge regions, as suggested by recent theoretical studies. In order to retain the structural information of the bridge and its anisotropic polarizability, the molecular linker is described through a classical polarizable MM force field. The solvent, conversely, can be described either using a classical MM description or a continuum solvation model. Moreover, a mixed solvent description can also be adopted, where only the first solvation shell is described explicitly, in order to retain specific solute-solvent interactions.

We have shown that the model is able to describe the bridge-mediated enhancement of the EET coupling in different dyads (such as perylene linked by phenyl-based spacers and porphyrins with a diaryl-ethyne linkers). We have also illustrated the limitations of the model which clearly cannot be applied to describe the bridge effect in systems where the bridge is strongly coupled to the donor moiety via charge transfer interactions.

Moreover, we have shown that both MM and PCM models provide a good description of solvent screening effects, and this choice should be considered depending on the system under study. While it is advantageous to model solvation through PCM in homogeneous media such as a standard solvent, an atomistic MM force field can improve the description of the environment in heterogeneous systems, such as organic crystals, polymers, or biological macromolecules. Indeed, in organic materials the separation between "bridge" and "environment" regions can be less straightforward, and thus a unified modeling of the whole system at the MM level allows to tackle both effects on an equal footing. Even in a homogeneous solvent, it can be interesting to include the first solvation shells at the MM level if strong specific solute-solvent interactions are expected to be important. An atomistic MM description can also be used to provide insights on the role of different structural regions of the system on the enhancement/screening of EET interactions, because the explicit environment-mediated contribution to the coupling can be dissected into atomic or group contributions, as we showed recently for a photosynthetic antenna complex.[22] On the other hand, a dielectric continuum description of the environment (solvent) can be advantageous whenever detailed structural information of the environment is missing, and prevents the need to perform molecular dynamics simulations of the system and subsequently a number of EET calculations in order to account for configurational sampling. Moreover, the easiness of continuum models to be extended to very different environments such as interfaces, membranes, as well as composite systems including metal nanoparticles,[53] makes this integration with a polarizable MM approach a very promising strategy to describe EET processes in systems of increasing complexity.

Acknowledgments

B.M. and S.C. acknowledge the European Research Council (ERC) for financial support in the framework of the Starting Grant (EnLight-277755). C.C. acknowledges support from the Spanish Ministry of Economy and Competitivity through the Ramón y Cajal program (Ref. RYC-2011-08918).

References

(1) Fleming, G. R.; Schlau-Cohen, G. S.; Amarnath, K.; Zaks, J. *Faraday Discussions* **2012**, *155*, 27–43.

(2) Scholes, G. D.; Fleming, G. R.; Olaya-Castro, A.; Van Grondelle, R. *Nature Chemistry* **2011**, *3*, 763–774.

(3) Novoderezhkin, V. I.; Van Grondelle, R. *Physical Chemistry Chemical Physics* **2010**, *12*, 7352–7365.

(4) Cheng, Y.-C.; Fleming, G. R. *Annual Review Of Physical Chemistry* **2009**, *60*, 241–262.

(5) Sariciftci, N. S.; Smilowitz, L.; Heeger, A. J.; Wudl, F. *Science (New York, N.Y.)* **1992**, *258*, 1474–1476.

(6) Halls, J.; Walsh, C.; Greenham, N.; Marseglia, E.; Friend, R.; Moratti, S.; Holmes, A. *Nature* **1995**, *376*, 498–500.

(7) Lee, J.; Kang, I.; Hwang, D.; Shim, H.; Jeoung, S.; Kim, S. *Chemistry of Materials* **1996**, *8*, 1925–1929.

(8) Wang, H.; McBranch, D.; Klimov, V.; Helgeson, R.; Wudl, F. *Chemical Physics Letters* **1999**, *315*, 173–180.

(9) Förster, T. *Ann. Phys. (Leipzig)* **1948**, *2*, 55.

(10) Speiser, S. *Chemical Reviews* **1996**, *96*, 1953–1976.

(11) Albinsson, B.; Martensson, J. *Journal of Photochemistry and Photobiology C-Photochemistry Reviews* **2008**, *9*, 138–155.

(12) Albinsson, B.; Mårtensson, J. *Phys. Chem. Chem. Phys.* **2010**, *12*, 7338–51.

(13) Newton, M. *Chemical Reviews* **1991**, *91*, 767–792.

(14) Jordan, K.; Paddon-Row, M. *Chemical Reviews* **1992**, *92*, 395–410.

(15) Hsu, C.-P.; Fleming, G. R.; Head-Gordon, M.; Head-Gordon, T. *J. Chem. Phys.* **2001**, *114*, 3065–3072.

(16) Curutchet, C.; Mennucci, B. *Journal Of The American Chemical Society* **2005**, *127*, 16733–16744.

(17) Adolphs, J.; Renger, T. *Biophysical Journal* **2006**, *91*, 2778–2797.

(18) Scholes, G. D.; Curutchet, C.; Mennucci, B.; Cammi, R.; Tomasi, J. *The Journal of Physical Chemistry B* **2007**, *111*, 6978–6982.

(19) Curutchet, C.; Muñoz-Losa, A.; Monti, S.; Kongsted, J.; Scholes, G. D.; Mennucci, B. *J. Chem. Theory Comput.* **2009**, *5*, 1838–1848.

(20) Neugebauer, J.; Curutchet, C.; Munoz-Losa, A.; Mennucci, B. *Journal Of Chemical Theory And Computation* **2010**, *6*, 1843–1851.

(21) Mennucci, B.; Curutchet, C. *Physical Chemistry Chemical Physics* **2011**, *13*, 11538–11550.

(22) Curutchet, C.; Kongsted, J.; Munoz-Losa, A.; Hossein-Nejad, H.; Scholes, G. D.; Mennucci, B. *Journal Of The American Chemical Society* **2011**, *133*, 3078–3084.

(23) Renger, T.; Müh, F. *Photosynthesis Research* **2012**, *111*, 47–52.

(24) Tretiak, S.; Zhang, W. M.; Chernyak, V.; Mukamel, S. *Proceedings of the National Academy of Sciences* **1999**, *96*, 13003–13008.

(25) Thompson, A.; Gaab, K.; Xu, J.; Bardeen, C.; Martinez, T. *The Journal of Physical Chemistry A* **2004**, *108*, 671–682.

(26) Russo, V.; Curutchet, C.; Mennucci, B. *The Journal of Physical Chemistry B* **2007**, *111*, 853–863.

(27) Curutchet, C.; Mennucci, B.; Scholes, G. D.; Beljonne, D. *J. Phys. Chem. B* **2008**, *112*, 3759–66.

(28) Fückel, B.; Köhn, A.; Harding, M. E.; Diezemann, G.; Hinze, G.; Basché, T.; Gauss, J. *J. Chem. Phys.* **2008**, *128*, 074505.

(29) Van Averbeke, B.; Beljonne, D.; Hennebicq, E. *Advanced Functional Materials* **2008**, *18*, 492–498.

(30) Chen, H.-C.; You, Z.-Q.; Hsu, C.-P. *J. Chem. Phys.* **2008**, *129*, 084708.

(31) Curutchet, C.; Feist, F. A.; Van Averbeke, B.; Mennucci, B.; Jacob, J.; Müllen, K.; Basché, T.; Beljonne, D. *Phys. Chem. Chem. Phys.* **2010**, *12*, 7378–7385.

(32) König, C.; Neugebauer, J. *Chemphyschem : a European journal of chemical physics and physical chemistry* **2012**, *13*, 386–425.

(33) Iozzi, M. F.; Mennucci, B.; Tomasi, J.; Cammi, R. *J. Chem. Phys.* **2004**, *120*, 7029–7040.

(34) Tomasi, J.; Mennucci, B.; Cammi, R. *Chem. Rev.* **2005**, *105*, 2999–3093.

(35) Cances, E.; Mennucci, B.; Tomasi, J. *The Journal of Chemical Physics* **1997**, *107*, 3032–3041.

(36) Mennucci, B.; Cances, E.; Tomasi, J. *The Journal of Physical Chemistry B* **1997**, *101*, 10506–10517.

(37) Steindal, A. H.; Ruud, K.; Frediani, L.; Aidas, K.; Kongsted, J. *The Journal of Physical Chemistry B* **2011**, *115*, 3027–3037.

(38) Cammi, R.; Mennucci, B. *J. Chem. Phys.* **1999**, *110*, 9877–9886.

(39) Yanai, T.; Tew, D.; Handy, N. *Chemical Physics Letters* **2004**, *393*, 51–57.

(40) Frisch, M. J. et al. Gaussian 09 Revision A.1. Gaussian Inc. Wallingford CT 2009.

(41) Sing, U. C.; Kollman, P. *J. Comput. Chem.* **1984**, *5*, 129–145.

(42) Besler, B. H.; Merz Jr, K. M.; Kollman, P. A. *J. Comput. Chem.* **1990**, *11*, 431–439.

(43) Senn, H. M.; Thiel, W. *Angew. Chem. Int. Ed.* **2009**, *48*, 1198–1229.

(44) Thole, B. T. *Chem. Phys.* **1981**, *59*, 341.

(45) van Duijnen, P. T.; Swart, M. *J. Phys. Chem. A* **1998**, *102*, 2399–2407.

(46) Wang, J.; Cieplak, P.; Li, J.; Hou, T.; Luo, R.; Duan, Y. *The Journal of Physical Chemistry B* **2011**, *115*, 3091–3099.

(47) Case, D. et al. AMBER 9, University of California, San Francisco, 2006.

(48) Wang, J.; Wolf, R. M.; Caldwell, J. W.; Kollman, P. A.; Case, D. A. *Journal Of Computational Chemistry* **2004**, *25*, 1157–1174.

(49) Métivier, R.; Nolde, F.; Müllen, K.; Basché, T. *Phys. Rev. Lett.* **2007**, *98*, 047802.

(50) Hsiao, J.-S.; Krueger, B. P.; Wagner, R. W.; Johnson, T. E.; Delaney, J. K.; Mauzerall, D. C.; Fleming, G. R.; Lindsey, J. S.; Bocian, D. F.; Donohoe, R. J. *Journal of the American Chemical Society* **1996**, *118*, 11181–11193.

(51) Jensen, K. K.; van Berlekom, S. B.; Kajanus, J.; Mårtensson, J.; Albinsson, B. *J. Phys. Chem. A* **1997**, *101*, 2218–2220.

(52) Strachan, J.-P.; Gentemann, S.; Seth, J.; Kalsbeck, W. A.; Lindsey, J. S.; Holten, D.; Bocian, D. F. *J. Am. Chem. Soc.* **1997**, *119*, 11191–11201.

(53) Mennucci, B. *Wiley Interdisciplinary Reviews-Computational Molecular Science* **2012**, *2*, 386–404.

TOC